Optimizing the Zel'dovich Approximation

Adrian L. Melott, Todd F. Pellman, and Sergei F. Shandarin
Department of Physics and Astronomy
University of Kansas
Lawrence, Kansas 66045 USA

ABSTRACT

We have recently learned that the Zeldovich approximation can be successfully used for a far wider range of gravitational instability scenarios than formerly proposed; we study here how to extend this range. In previous work (Coles, Melott and Shandarin 1993, hereafter CMS) we studied the accuracy of several analytic approximations to gravitational clustering in the mildly nonlinear regime. We found that what we called the "truncated Zel'dovich approximation" (TZA) was better than any other (except in one case the ordinary Zeldovich approximation) over a wide range from linear to mildly nonlinear ($\sigma \sim 3$) regimes. TZA was specified by setting Fourier amplitudes equal to zero for *all* wavenumbers greater than $k_{n\ell}$, where $k_{n\ell}$ marks the transition to the nonlinear regime. Here, we study the crosscorrelation of generalized TZA with a group of n–body simulations for three shapes of window function: sharp k–truncation (as in CMS), a tophat in coordinate space, or a Gaussian. We also study the variation in the crosscorrelation as a function of initial truncation scale within each type.

We find that k–truncation, which was so much better than other things tried in CMS, is the *worst* of these three window shapes. We find that a Gaussian window $e^{-k^2/2k_G^2}$ applied to the intial Fourier amplitudes is the best choice. It produces a greatly improved crosscorrelation in those cases which most needed improvement, e.g. those with more small–scale power in the initial conditions. The optimum choice of k_G for the Gaussian window is (a somewhat spectrum–dependent) 1 to 1.5 times $k_{n\ell}$, where $k_{n\ell}$ is defined by (3). Although all three windows produce similar power spectra and density distribution functions after application of the Zeldovich approximation, the agreement of the phases of the Fourier components with the n–body simulation is better for the Gaussian window. We therefore ascribe the success of the best–choice Gaussian window to its superior treatment of phases in the nonlinear regime. We also report on the accuracy of particle positions and velocities produced by TZA.

Key Words: galaxies:clustering–cosmology:theory–large–scale structure of the Universe

1 INTRODUCTION

For nearly fifty years there has been interest in understanding the gravitational growth of density perturbations in an expanding universe. For the latter half of this time, we have seen increasingly sophisticated numerical simulations performed on increasingly powerful computers in an attempt to model this process. There has been a fruitful interaction with theory; much of the effort has gone into two directions: (a) does a particular scenario produce something that looks like our universe? (b) what approximations can we develop to describe the general properties of the clustering process? This paper lies in second of these traditions.

The Zel'dovich (1970) approximation is the focus of this paper. One of us (ALM) suggests there are strong indications near the end of section 3 that he thought this approximation might work for entropic perturbtions (hierarchical clustering). However, it quickly was decided in a later paper (Zel'dovich 1973) that it would work only to describe Universes in which large wavelength perturbations dominate, which were associated with what was then called the "adiabatic" picture or sometimes the "pancake" model, after the large flattened structures that appeared in it.

During the 80's, evidence gradually accumulated that the approximation had wider validity. Filamentary structure appeared in a variety of numerical simulations, beginning with CDM when Melott *et al.* (1983) found that it had enhanced percolation.

Coles, Melott and Shandarin (1993) hereafter CMS, conducted a series of tests by crosscorrelating n–body simulations with various approximate solutions to the same initial conditions. They found the Zel'dovich approximation, particularly in a "truncated" form implemented by smoothing the initial conditions to remove unwanted nonlinearity, was the most successful. The idea of the truncation of the initial spectrum evolved from the very well known linear theory to the comparison of N–body simulations having the same longwave perturbations but different cutoffs as in Beacom *et al.* (1991) and Melott and Shandarin (1993) then to the adhesion approximation as in Kofman *et al.* (1992), and of the truncated Zeldovich approximation (CMS). In this paper we improve on that success by finding the best way to do the initial smoothing. We will see that a considerable further improvement is made.

We first define a dimensionless density contrast $\delta(\mathbf{x})$ for the matter density ρ in co–moving coordinates $\mathbf{x} = \mathbf{r}/a(t)$ by

$$\delta(\mathbf{x},\mathbf{t}) = \frac{\rho(\mathbf{x},\mathbf{t}) - \rho_0}{\rho_0} \tag{1}$$

$a(t)$ is the cosmological scale factor and, assuming a flat Universe with $\Omega_0 = 1$ and in the absence of radiation and pressure terms, $a(t) \propto t^{2/3}$ and $\rho_0(t) \propto a^{-3} \propto t^{-2}$. The evolution of $\delta(\vec{\mathrm{x}}, t)$ is described by the standard set of equations (e.g. Peebles, 1980 Eq. (7.9) and (9.1)).

Furthermore, we specify the following initial conditions. If δ_k is the spatial Fourier transform of the density contrast (1), then our scale–free initial perturbations are expressed by a power spectrum of the form

$$P(k) = <\mid \delta_k \mid^2> \propto k^n \ . \tag{2}$$

In the following discussion we will take $n = +1, 0, -1, -2$ for illustrative examples. At the initial time when the density contrast is everywhere small we assume that phases of the Fourier components are randomly distributed on the interval [0,2π]. In this case, $\delta(\mathrm{x})$ is a Gaussian random field and all of its statistical properties are completely contained in the power spectrum (2).

In Fourier space, components δ_k for large magnitudes k correspond to structure on small scales and similarly for small k and large structures. We define k–nonlinear, or $k_{n\ell}$, by

$$a^2(t) \int_0^{k_{n\ell}} P(k) d^3\mathrm{k} = 1 \ . \tag{3}$$

With this definition of $k_{n\ell}$ we can say that for $k < k_{n\ell}$ we are considering structures in the linear regime, that is, structures whose density contrasts have grown approximately proportional to $a(t)$. Clearly, $k_{n\ell}$ decreases with time as larger scales become more nonlinear.

2 A GENERALIZED TRUNCATED ZELDOVICH APPROXIMATION

With the Zeldovich approximation (Zeldovich 1970) we simply assign to each material particle (strictly to the particle's initial unperturbed Lagrangian co–ordinate $\mathbf{q}$) a vector and move the particle along that vector. The Eulerian (co–moving) coordinate $\mathbf{x}$ of a particle at time t is given by

$$\mathbf{x}(\mathbf{q}, t) = \mathbf{q} + a(t) \nabla \Phi_i(\mathbf{q}) \tag{4}$$

where $\Phi_i(\mathbf{q})$ is the initial *velocity potential*, related to the initial gravitational potential by

$$\phi_i(\mathbf{x}) = -\frac{3}{2} H^2 a^3 \Phi_i(\mathbf{x}) \tag{5}$$

so that $\nabla^2 \Phi_i \propto \delta$ and the approximation is readily obtained from the initial conditions (2).

The *ansatz* (4) leads to a catastrophe where trajectories cross, a phenomenon known as shell crossing (e.g., Shandarin & Zeldovich 1989). However, until the catastrophe is reached, the approximation performs well, but only for $n \leq -3$, i.e., for spectra in which most of the power is concentrated on large scales. This effect can be easily understood when one considers that it is on small scales that the highly nonlinear effects occur. Thus, we can expect to improve upon the approximation (4) by first damping out initial power for large k, i.e., small scales. We call this the "truncated Zel'dovich" approximation, or TZA.

We investigate here the effect of three "windows" applied in Fourier space. That is, for a window $W(k)$ the initial conditions δ_k^* for the improved approximation are just $\delta_k^* = W(k)\delta_k$ where δ_k are the initial conditions as given before (2). Since the phases of the coefficients are not changed, we will be able to test directly the agreement.

The window which we will refer to as k–truncated is simply

$$W_{tr}(k; k_{tr}) = \begin{cases} 1, & k \leq k_{tr} \\ 0, & k > k_{tr} \end{cases} \tag{6}$$

This has already been shown to be an improvement to the original approximation (CMS), however, it was only investigated for $k_{tr} = k_{n\ell}$. Here we tested it for a range from $k_{tr} = 2k_f$ to $k_{tr} = 20k_f$ where k_f is the fundamental mode of the box at two stages: $k_{n\ell} = 8k_f$ and $k_{n\ell} = 4k_f$.

The other two windows tested are a Gaussian window

$$W_G(k; k_G) = e^{-k^2/2k_G^2} \tag{7}$$

and a top–hat window in real space which corresponds in Fourier space to

$$W_{th}(k; R_{th}) = 3\left(\frac{\sin R_{th}k}{(R_{th}k)^3} - \frac{\cos R_{th}k}{(R_{th}k)^2}\right) \tag{8}$$

We similarly tested these windows over a range of k_G and R_{th} to find the parameters for the best performance. The meaning of "best" will be clarified in section 4.

We investigated a fourth window defined by

$$W(k; k^*) = \begin{cases} 1, & k \leq k^* \\ e^{-k^2/2k^{*2}}, & k > k^* \end{cases} \tag{9}$$

motivated by the need to suppress small scale power in a gradual fashion and the belief that the Zeldovich approximation worked well for large scale power and so we should leave

those amplitudes unaffected. However, this window performed only slightly better than k–truncated so we do not consider it further.

3 NUMERICAL SIMULATIONS

The model data to which we compare the TZA approximations is provided by a set of N–body experiments that approximate the evolution of a cosmological density field with a set of particles on a grid with periodic boundary conditions. The details are discussed much more completely by CMS and in Melott and Shandarin (1993) hereafter MS; the essentials of such a simulation are the following.

Each N–body simulation is evolved from a set of initial density fluctuations with power spectra of the form (2) and random phases. At very low amplitude our use of the Zeldovich approximation (4) for initial conditions generates not only particle displacements but also velocities in accord with the growing mode of gravitational instability. The initial low amplitude restriction was such that no particle could be displaced more than 1/2 the cell width from homogeneity. We studied spectra corresponding to $n = 1, 0, -1, -2$, all generated from the same set of random phases, which explains the similar overall structures of simulations with different spectra. The simulations were run for various expansion factors $a(t)$; we consider here only those stages corresponding to $k_{nl} = 8k_f$ and $k_{nl} = 4k_f$. These two scales represent a good compromise between resolution in terms of particles which drives one to large scales and the effect of our periodic boundary conditions which leads one to small scales (Kauffmann & Melott 1992).

For all cases, N–body and various versions of TZA, we evolved 128^3 particles, each on a 128^3 co–moving mesh with periodic boundary conditions. For the N–body results we used the enhanced PM (particle–mesh) method of Melott (1986). This makes them resolution equivalent to simulations with 128^3 particles on a 256^3 grid in traditional PM codes: see also Park (1990, 1991) and Weinberg et al. (1993). Grey scale plots of thin slices through these densities corresponding to $k_{nl} = 8$ are shown in Figures 1a, 2a, 3a, and 4a for the N–body simulations.

4 CROSS CORRELATIONS

As in CMS we use here the usual cross–correlation coefficient to compare each grid–point in the resulting TZA approximations to the corresponding grid–point in the N–body simulation. This coefficient is given by

$$S = \frac{< (\delta_1 \delta_2 >}{\sigma_1 \sigma_2} \tag{10}$$

where δ_1 and δ_2, represent the density contrasts in the TZA and N–body distributions, respectively; $\sigma_i \equiv < \delta_i^2 >^{1/2}$; and averages are over the entire distribution. Note $\mid S \mid \leq 1$ and that $S = +1$ implies that $\delta_1 = C\delta_2$, with C constant for every pixel.

We exploit our use of identical phases before n–body evolution or application of an approximation to demand good agreement. Our crosscorrelation test would be impossible without it.

CMS found that the cross correlations between TZA and N–body for different realizations of the random phases agreed to the order of 10^{-3}. This allows us to make general conclusions about the performance of an approximation from our investigation of only one realization.

The cross–correlation technique applied to the "raw" density fields may be too strict a test. If the relative position of the structure is very similar to the N–body results but is slightly displaced from those of the N–body, a small cross–correlation can result. We can overcome this by smoothing the resulting density fields by a convolution with a Gaussian:

$$\delta(\mathrm{x}, R) = \frac{1}{\left(\sqrt{2\pi}R\right)^3} \int \delta(\mathrm{x}') \exp\left(\frac{-\mid \mathrm{x} - \mathrm{x}' \mid^2}{2R^2}\right) d^3\mathrm{x}' \ . \tag{11}$$

Thus, the question becomes not how well do two density fields correlate, but how fast do the correlations converge to unity with smoothing?

Fields evolved from different values of n will respond differently to a given smoothing length R, so we find it more convenient to express S as a function of the rms density contrast σ. This is somewhat more intuitive; σ goes to zero as the field is more smoothed and S goes to unity.

We found when doing these crosscorrelations that there was no ambiguity in the ordering of windows; the rank–ordering of the crosscorrelations did not change with smoothing lengths for a given window size. We were thus able to explore a wide variety of values for the three window scales k_{tr}, k_G, and k_{th}. (Although the tophat window is more naturally represented by a smoothing radius R_{th}, for uniformity of notation we choose to use $k_{th} = 1/R_{th}$ to represent it.)

5 RESULTS AND DISCUSSION

All window functions had a single, fairly broad maximum crosscorrelation for a preferred value of k. We used the TZAs to generate a mass distribution for this choice of best

value for each window, and made plots of them in analogy with the n–body plots. These are shown in Figures 2, 3, and 4. Each Figure contains one n–body simulation and the three forms of TZA we compare with it.

All the pictures have a family resemblance, as expected. The arrangement of the pictures in a square array allows the reader to easily compare appearance across approximations. As usual, more negative n leads to a more filamentary appearance in all cases and for all indices the various versions TZA exaggerates the filamentarity. This is because the TZA cannot follow in detail the highly nonlinear process of the breakup of filaments into subclumps. The visual differences between the versions of TZA are more subtle. They resemble each other more for more negative n; this is reasonable since they differ primarily in the treatment of larger wavenumbers in the initial conditions and these are less important for more negative n. Within a given index, the Gaussian window appears to produce a picture which has a more "smooth" or "regular" appearance, whereas the others give an impression of "choppiness" or "irregularity". Also in the Gaussian version both the dark condensations and the grey filaments connecting them appear more compact.

In Figure 5 we demonstrate the best–choice scale k_w for each window in units of $k_{n\ell}$. The first thing we notice is that the optimum window value k_w is nearly the same for the two nonlinear stages (open and filled symbols in Figure 5), reinforcing the fact that our results are not limited by resolution or boundary conditions. Figures 2–4 show the stage $k_{n\ell} = 8k_f$ which allows us to see more structure within one slice.

Figure 5 shows the range of best k_w for our three window functions. The small disagreement seen between the two stages is an artifact of the fact that we only checked certain discrete values of k_w. The fact that the best value of k_w varies only a little for a given window over the range of indices (the greatest being a factor of about 5/3 for k–truncation), combined with the fact that we found that $\pm 20\%$ error in k_w makes very little difference, suggests that it will be possible to state a general prescription good for all kinds of spectra.

Figure 6 shows the crosscorrelations between the n–body simulations and our best choice k_w approximations for various spectra at both stages. Again all the dependence on particulars of the simulation box are removed by plotting against σ of the smoothed simulation. Each point is generated by crosscorrelating the n–body and the approximation both smoothed by convolution with the same Gaussian windows. This smoothing of our results should not be confused with the window function applied to the initial conditions.

We can now compare the best results for each window against one another. (The reader may also refer to Figure 6 in CMS.) The reader should note that the crosscorrelation has no absolute meaning; the raw number depends on the pixellization size relative to the size of structures after smoothing, and this is different at the two stages. But the relative order should stay the same, and does. A value of 1 would mean perfect agreement at the resolution of one pixel, even if mass were rearranged inside pixels. CMS used the same pixels, so that can be directly compared to results here for the same $k_{n\ell}$ an spectral index.

For all eight panels in Figure 6, the Gaussian window produces the strongest cross-correlation between the resulting TZA density and that from the n–body simulation. The k–truncation method, which was so successful compared with other things tried by CMS, is the worst here. The greatest amount of improvement found by CMS for TZA over straightforward use of the Zeldovich approximation ($W = 1$) was found for more positive indices. We find here that the transition to a Gaussian window also makes the greatest increment in S beyond the CMS result for more positive indices. For $n = 1$, $\sigma = 1$, the value found by CMS was about 0.65; here it is about 0.85.

Returning to Figure 5 momentarily, we observe that the best value of $k_G/k_{n\ell}$ varies rather slowly with spectral index, lying in the range 1 to 1.5. One may be concerned about how to apply this to non–power law spectra such as Cold Dark Matter. We speculate that the local slope at $k_{n\ell}$ will determine this, and plan a check in the future. However, given the fact that $\pm 20\%$ in k_G makes little difference, we can recommend generic use of $k_w \sim 1.25 k_{n\ell}$ for non–power law spectra in which all of the quasilinear regime of the spectrum lies in the range $-2 \leq n \leq +1$. This includes nearly all models of cosmological interest at this time. Modes $k << k_{n\ell}$ will be unaffected by our window, and modes $k > 3k_{n\ell}$ will be damped to insignificance.

We can speculate based on the pictures why the Gaussian window works best. The first crisis and failure of any Zeldovich approximation–based scheme happens when trajectories cross. In real nonlinear gravity, the particles are slowed by the attraction of the stream they have passed, which is ignored in the approximation. This forces us to take out highly nonlinear modes. On the other hand, they can help to preserve detail. It appears that the Gaussian window works to balance these, reducing the amplitude of the more nonlinear modes gradually as they begin to lead mass elements further astray. This can account for the more focused and crisp appearance of the Gaussian based pictures.

The Zeldovich approximation does not conserve either the power spectrum or phases of Fourier components; it definitely includes some nonlinear mode coupling. It is therefore useful to examine the agreement with the n–body simulation. The power spectrum (or autocorrelation) is the most widely used statistic in large–scale structure. We examine that first without additional smoothing after applying TZA, in Figure 7. In all cases, the nonlinear power is too low in all approximate schemes. The other obvious point is that the spectra of the nonlinear approximations for a given model are all very similar in spite of the fact that their progenitors had different spectra. This is a reflection of the fact that the nonlinear transfer of power from small to large wavenumbers is dominant, as has been observed before. More importantly for our purposes here, it shows us that the better agreement of the Gaussian TZA cannot be a result of a spectrum closer to the n–body result. In fact, for $n = -1$ initial conditions, its spectrum is one of the farthest from the n–body result.

We therefore look to phase differences. Each Fourier coefficient in the sum that describes our density field has an amplitude and a phase angle α : $\delta_{\mathbf{k}} =\mid \delta_{\mathbf{k}} \mid e^{i\alpha}$. We can measure the angle $\theta = \alpha_N - \alpha_Z$ between the phases in the n–body simulation and the approximation to it. Perfect agreement would imply $\cos\,\theta = 1$; anticorrelation of phases $\cos\,\theta = -1$; and for randomized phases $\cos\,\theta$ would average 0. We expect the phase agreement to deteriorate with increasing k; we thus average $\cos\,\theta$ within spherical shells of k and plot $< \cos\theta >$ as a function of k in Figure 8. The results are in agreement with our crosscorrelation study: the Gaussian based approximation has phases which agree the best with those of the n–body simulation, and this agreement is weakly if at all spectrum dependent. The k–truncation based approximation is the worst and the most spectrum dependent. This is in perfect accordance with the fact that we have improved TZA and greatly reduced its spectral dependence by using a Gaussian window, and reinforces the importance of phase information as stressed by Scherrer et al. (1991), Ryden and Gramman (1991), and Howe (1993).

We can understand the performance a little better by examining the density distribution function. In Figure 9 we show the number of cells N found with mass density ρ (in units of the mean). In all cases the approximations underestimate the number of high density cells and overestimate the number of lower density cells. We can also see that there is no systematic difference between the windows. Therefore the difference in crosscorelation amplitude must depend primarily on producing the correct location of mass condensations, rather than substantial differences in their density contrast.

It is worth commenting that our results do not imply that Gaussian smoothing is the best for restoring initial conditions from our nonlinear universe with the Zeldovich approximations; smoothing does not commute with the approximation. Melott (1993) has shown that if one wishes to smooth an evolved state in preparation for computing its linear precursor, then k–truncation works best. This is probably because the sharp truncation effectively removes nonlinearly generated modes which are of higher order than the Zeldovich approximation and would thus create a false signal when mapping back to the initial conditions; the signal would be false regardless of their amplitude. When extrapolating forward, as we are studying here, the effect of "sticking" in pancakes can apparently be mimicked by a gradual reduction of amplitude with increasing k.

Although we have conducted a fairly broad search, there are an infinite number of possible smoothing windows and we cannot exclude the possibility that some untried one would be even better than Gaussian. But it seems that finding it would be difficult if not impossible without a specific prediction based on theory.

A substantial improvement now exists as compared with linear theory, as one can see by comparing the crosscorrelation amplitudes we get from Gaussian TZA with those derived from linear theory. For the most challenging $n = +1$ spectra, we improve the correlation from 0.6 to 0.85 at $\sigma_\rho = 1$ and from about 0.4 to better than 0.75 at $\sigma_\rho = 2$. For $n = -1$, close to the slope on scales going nonlinear today, we see an improvement from 0.85 to about 0.95 for $\sigma_\rho = 1$, and from 0.75 to 0.85 for $\sigma_\rho = 2$. We have removed much of the spectrum dependence found in the CMS version of TZA, and it is now much better than linear theory for all spectral indices.

Much of the analytic theory of large–scale structure is based on the idea of smoothing to linearity, then using linear perturbation theory or simple extensions of it. Our results show that any calculations which can be based on TZA will be in much closer agreement with reality.

After this paper was submitted, we completed similar analyses of the frozen–flow approximation (Melott *et al.* 1994a) and the adhesion approximation (Melott *et al*, 1994b). Although these are considerably more complicated, they both crosscorrelated substantially worse than TZA. The adhesion approximation was better for some statistical quantities such as the mass density distribution function and the power spectrum, but worse dynamically in the sense of moving mass to the right place.

Second–order Lagrangian perturbation theory (ZA may be considered as first order) has recently been found by Melott *et al.* (1994c) to constitute a slight improvement over TZA, *if* the initial conditions are truncated by an optimal Gaussian smoothing. The improvements over first–order TZA are rather small; it is a question of taste whether it is worth the moderate complication.

We have not yet completed a similar analysis of the linear evolution of potential approximation (Brainerd *et al.* 1994; Bagla and Padmanaban 1994). This might do rather well. However, we wish to point out that this is not really an analytic nonlinear approximation, but rather a different way of doing N–body simulations. It consists of moving particles around over timesteps while assuming that the background potential is content, *i.e.*, evolves according to linear perturbation theory. In practice this is almost as expensive as doing a full N–body simulation, and it cannot be done analytically. It is therefore not directly comparable with TZA, which can be written analytically and executed in what is equivalent to one timestep of an N–body simulation.

Since TZA works so well, at the request of a referee we have also examined the distribution of errors in particle positions and velocities as compared with N–body. We define the position error

$$\Delta x = \frac{\mid \bar{\mathbf{x}}_{TZA} - \bar{\mathbf{x}}_{N-b} \mid}{\lambda_{n\ell}} \tag{12}$$

where $\lambda_{n\ell}$ is the nonlinearity wavelength. Figure 10 shows a histogram of Δx. A typical position error is spectrum dependent: $\Delta x \sim 0.15\lambda_{n\ell}$ for $n = +1$ and $\Delta x \sim 0.075\lambda_{n\ell}$ for $n = -2$, which is in a good qualitative agreement with all previous results.

The velocity field is a resolution – dependent quantity, and cannot be reported independent of some assumed smoothing window. In most practical applications, approximations like TZA are used in the quasi–linear regime, between the domain of validity of Eulerian perturbation theory and the fully nonlinear regime best handled by N–body simulations. We therefore choose to bin the velocities to define a center–of–mass velocity for our 128^3 density pixels. This density field is then smoothed by a Gaussian (11) for which the resulting RMS density contrast is unity. This is an extremely stable measure (about $R = 4h^{-1}$ Mpc for galaxy data). We report

$$\Delta v = \frac{\mid \bar{\mathbf{v}}_{TZA} - \bar{\mathbf{v}}_{N-b} \mid}{H\lambda_{n\ell}} \tag{13}$$

where H is the Hubble expansion parameter at the moment under analysis. In Figure 11 we show the distribution of Δv, weighted by mass. The dependence on spectrum is much

weaker than in the position error. Since both position and velocity errors are given in dimensionless (nautral) units they can be compared with each other. The velocity errors are considerably smaller, which probably can be related to the smoothing of the velocity distribution. In passing we note that the Zeldovich approximation itself is more accurate in terms of velocities than coordinates (Doroshkevich, Ryabenkii, and Shandarin (1973).

7 CONCLUSIONS

We have conducted a controlled study of the truncated Zeldovich approximation, which CMS found worked in a spectrum–dependent fashion but always better than linear theory. The TZA approximation consists of multiplying the linear Fourier coefficients by a window function $W(k/Ck_{n\ell})$ where C is a constant to be determined and $k_{n\ell}$ marks the transition to the nonlinear regime. We explored three shapes for the function W: a step function, a Gaussian, and the Fourier transform of a tophat (uniform sphere) and we varied C for each W.

We found that:

(a) A Gaussian window $e^{-k^2/2k_G^2}$ produces the best crosscorrelation with n–body simulations.

(b) The best choice for C for a Gaussian window is in the range 1 to 1.5, depending on the spectral index of the initial conditions, but very little error will be introduced by using 1.25 for all cases in the range $-2 \leq n \leq 1$.

(c) Using this window dramatically improves the performance for the more challenging positive–n case, removing much of the spectral dependence found in CMS.

(d) The reason for better performance of the Gaussian window is based on more nearly correct phases of Fourier coefficients in the nonlinear regime, whereas the power spectrum and the density distribution function produced are nearly the same for all windows. Visually all windows produce quite similar distributions.

(e) The use of TZA still considerably underestimates the power at large $k(k > k_{n\ell})$ and the density counts at high densities ($\rho \gtrsim 6$).

ACKNOWLEDGEMENTS

We are grateful for the financial support of (USA) NSF grants AST–9021414, OSR–9255223, and NASA grant NAGW–2923, which made this work possible. One of us (TP) is especially grateful from NSF Research Experiences for Undergraduates supplemental grant.

Our large–scale computations were performed on a Cray–2 and a Convex C3 at the National Center for Supercomputing Applications, Urbana, Illinois, USA.

REFERENCES

Bagla, J.S., and Padmanabhan, T., 1994 MNRAS, in press.

Beacom, J., Dominik, K., Melott, A., Perkins, S., and Shandarin, S., 1991, ApJ 372, 351

Brainerd, T.G., Scherrer, R.J., and Villumsen, J.V., 1994, ApJ in press

Coles, P., Melott, A.L., and Shandarin, S.F., 1993, MNRAS 260, 765

Doroshkevich, A.G., Ryabenkii, V.A., and Shandarin, S.F., 1973, Astrophysics 9, 144

Howe, N.R., 1993, PhD Thesis, Princeton

Kofman, L., Pogosyan, S., Shandarin, S.F., and Melott, A.L., 1992, ApJ 393, 437

Kauffmann, G., and Melott, A.L., 1992, ApJ 393, 415

Melott, A.L., 1993, ApJ Lett, 414, L73

Melott, A.L., 1986, Phys. Rev. Lett. 56, 1992

Melott, A.L., Einasto, J., Saar, E., Suisalu, I., Klypin, A.A., and Shandarin, S.F., 1983, Phys. Rev. Lett. 51, 935

Melott, A.L., Lucchin, F., Matarrese, S., and Moscardini, L., 1994a, MNRAS 000,000

Melott, A.L., and Shandarin, S.F., 1993, ApJ 410, 469

Melott, A.L., Shandarin, S.F., and Weinberg, D.H., 1994b, ApJ in press

Melott, A.L., Buchert, T., and Weiss, A., 1994c, Astron. Ap., in preparation

Melott, A.L., and Shandarin, S.F., 1993, ApJ 410, 469

Park, C., 1990, PhD Thesis, Princeton

Park, C., 1991, MNRAS 251, 167

Ryden, B., and Grammann, M., 1991, ApJ 383, L33

Scherrer, R.J., Melott, A.L., and Shandarin, S.F., 1991, ApJ 377, 29

Shandarin, S.F., and Zeldovich, Ya.B., 1989, Rev.Mod.Phys. 61, 185

Weinberg, D., et al., 1993, in peparation

Zeldovich, Ya.B., 1970, A&A 5, 84

Zeldovich, Ya.B., 1973, Astrophysics 6, 164

FIGURE CAPTIONS

Figure 1. A grayscale plot of thin ($L/128$) slices of the simulation cube, and the approximations to it for index $n = +1$ initial conditions at stage $k_{n\ell} = 8$. (a) the n–body simulation (b) the k–truncated TZA approximation (c) the tophat–truncated TZA model (d) the Gaussian–truncated TZA model.

Figure 2. As in Figure 1, but for $n = 0$ initial conditions.

Figure 3. As in Figure 1, but for $n = -1$ initial conditions.

Figure 4. As in Figure 1, but for $n = -2$ initial conditions.

Figure 5. A plot of the value of $k_w/k_{n\ell}$ which gave the best crosscorrelation for each choice of window function. The solid figures are for stage $k_{n\ell} = 4k_f$ the open for stage $k_{n\ell} = 8k_f$. The hexagons represent the value for the tophat window, the squares the gaussian window, and the triangles the k–truncation window. Many open figures are apparently missing because they coincide with the same figure filled.

Figure 6. A plot of the crosscorrelation S as defined in the text between the best TZA generated density field (Figs. 2–4) and the full n–body simulations against the rms density fluctuation in the simulation. Both are smoothed by the same Gaussian window. Solid line: Gaussian window. Dot–dashed line: tophat window. Dashed line: k–truncation (a) for $k_{n\ell} = 8k_f$ (b) for $k_{n\ell} = 4k_f$.

Figure 7. Power spectra for the various n–body simulations at $k_{n\ell} = 8k_f$ (heavy solid line) and for the best TZA with the k–truncation window (dashed line), tophat window (dot–dashed line) and Gaussian window (solid line).

Figure 8. The average effective phase angle error for each of the three windows, as measured by $< \cos\theta >$ as described in the text, all at stage $k_{n\ell} = 8k_f$. Simulation with $n = +1$: short–long dash line. $n = 0$: short dash. $n = -1$: long dash. $n = -2$: dot–short dash.

Figure 9. The mass density distribution in terms of the number of cells N with density ρ in units of the mean density, with CIC binning of 128^3 particles on our 64^3 mesh.

Figure 10. A histogram of the difference in position for identical particles as evolved by TZA or by n–body, divided by $\lambda_{n\ell}$.

Figure 11. A histogram of the difference in velocity for identical particles as evolved by TZA or by n–body, divided by $H(z)\lambda_{n\ell}$.

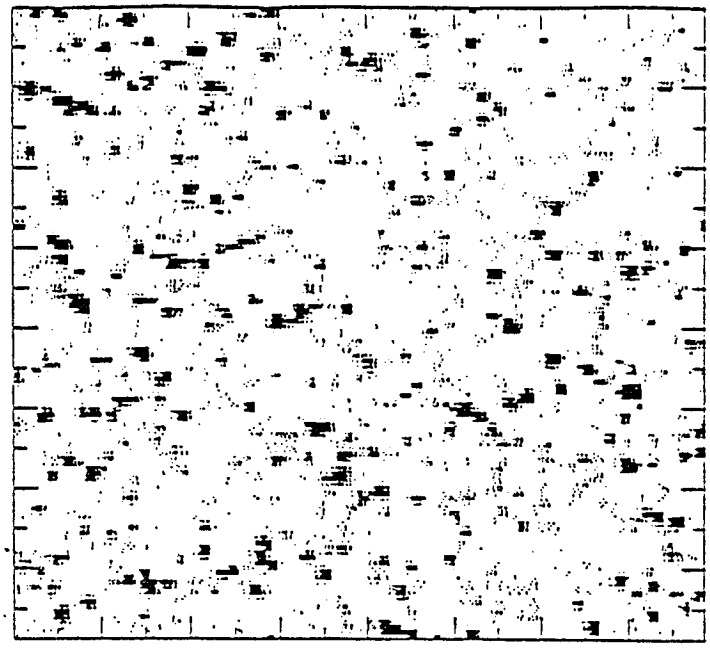

Fig. 1a

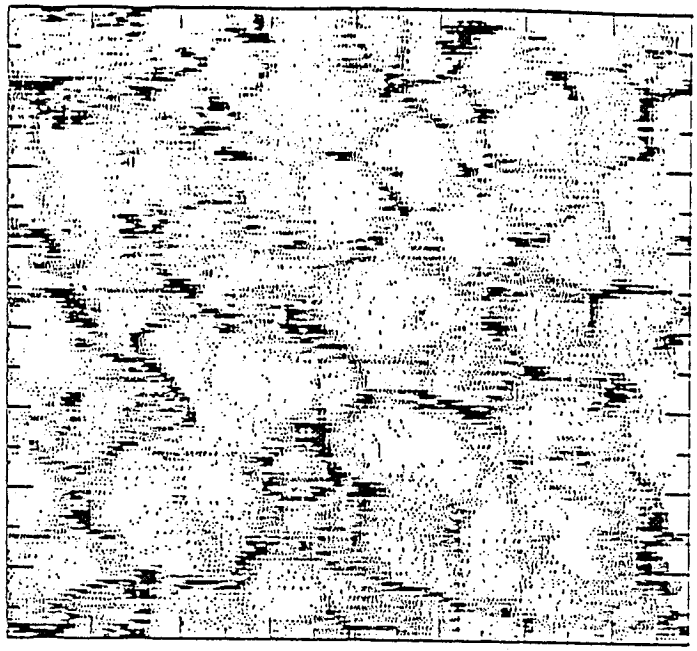

.Fig. 1b

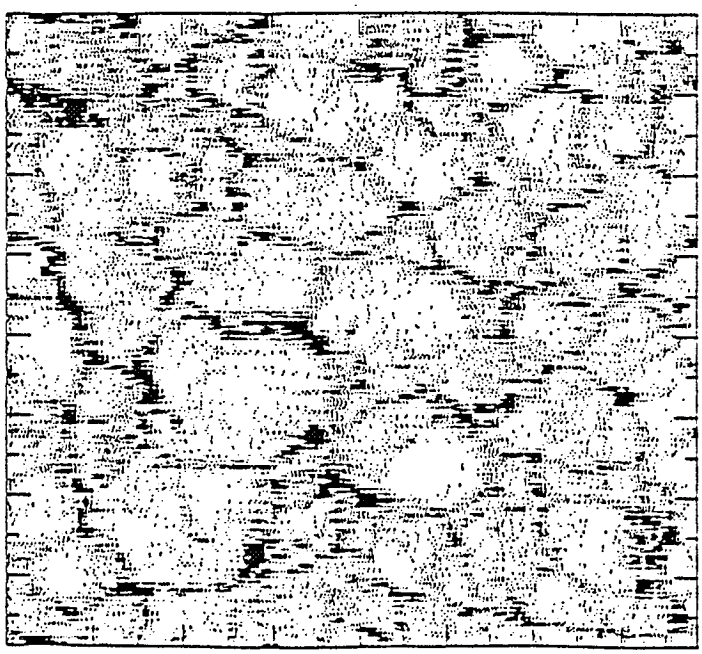

Fig. 1c

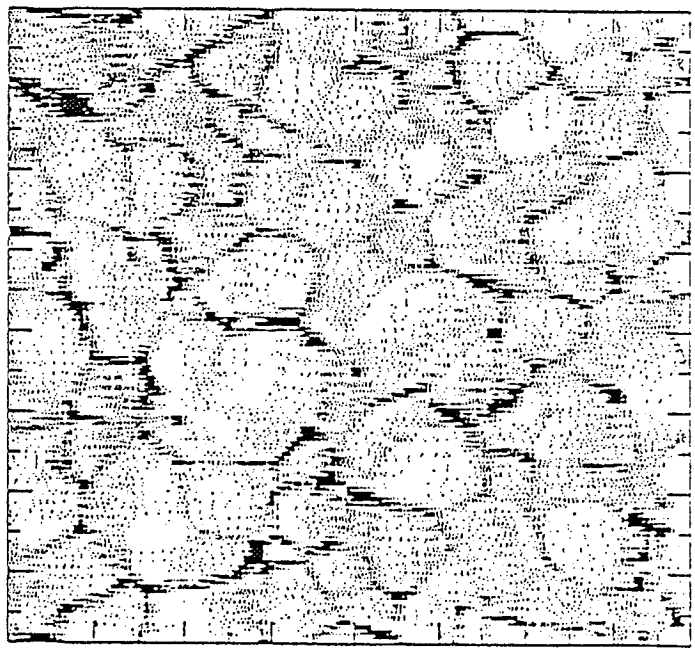

Fig. 1d

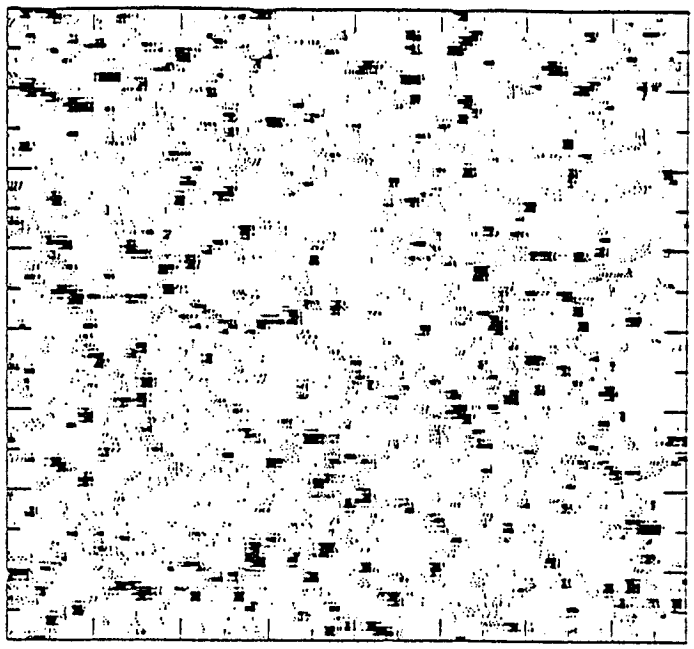

Fig. 2a

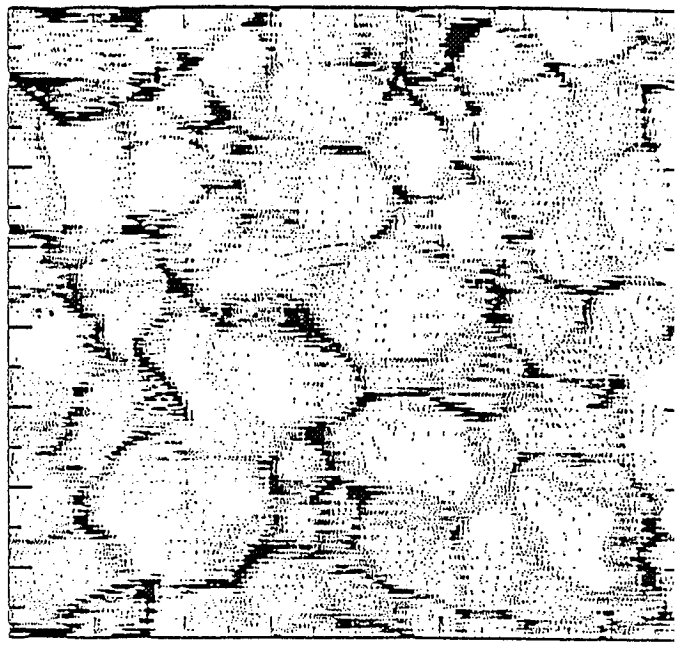

Fig. 2b

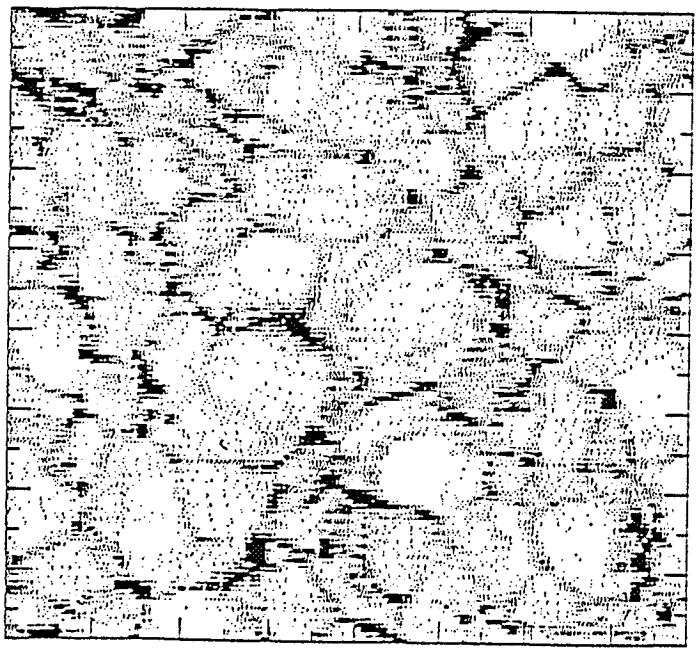

Fig. 2c

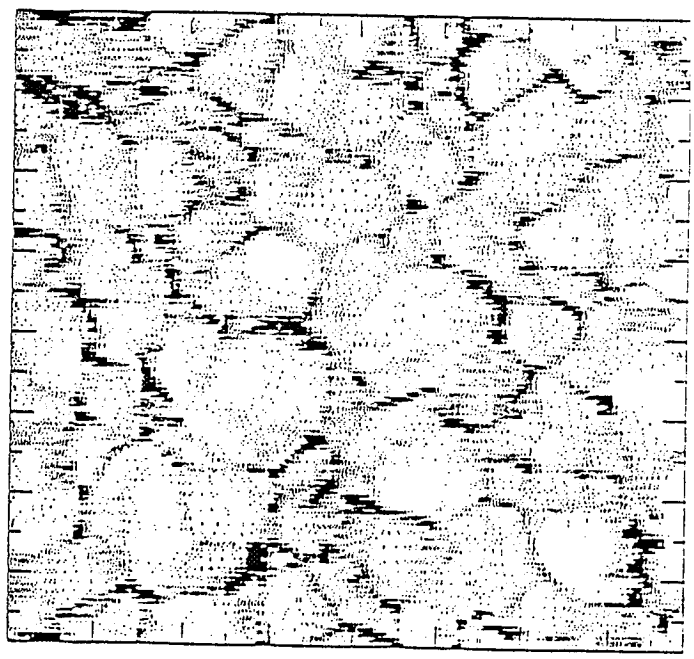

Fig. 2d

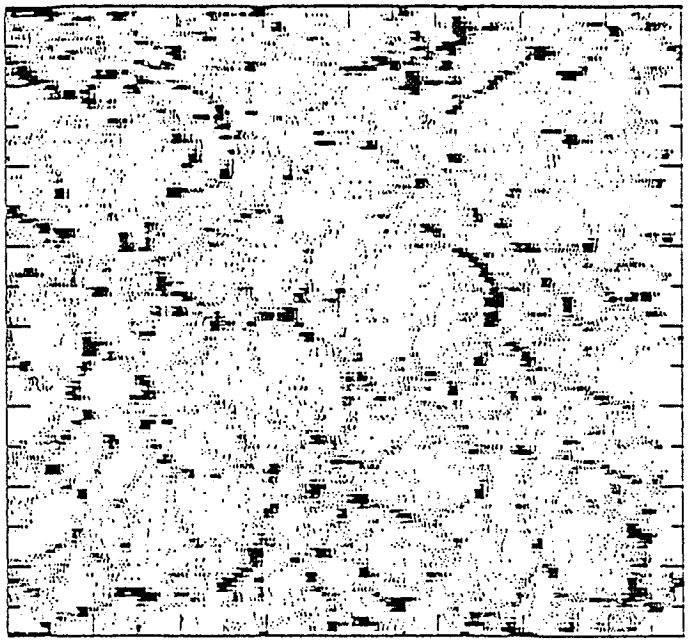

Fig. 3a

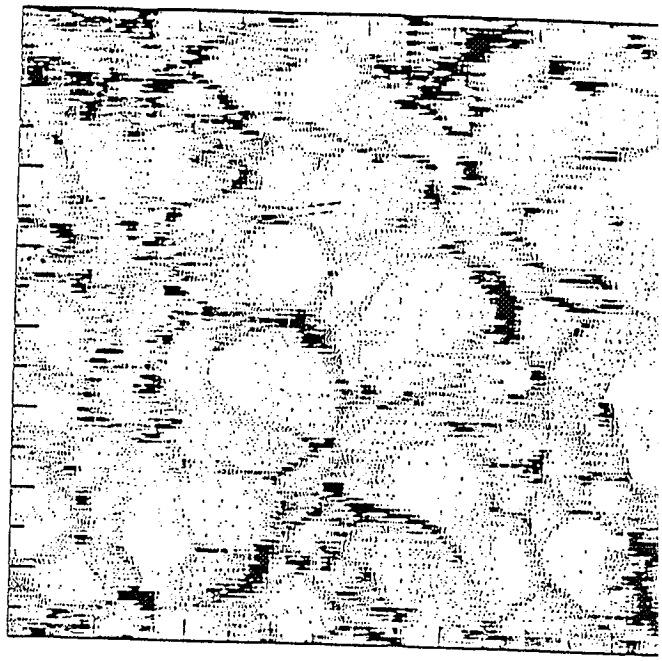

Fig. 3b

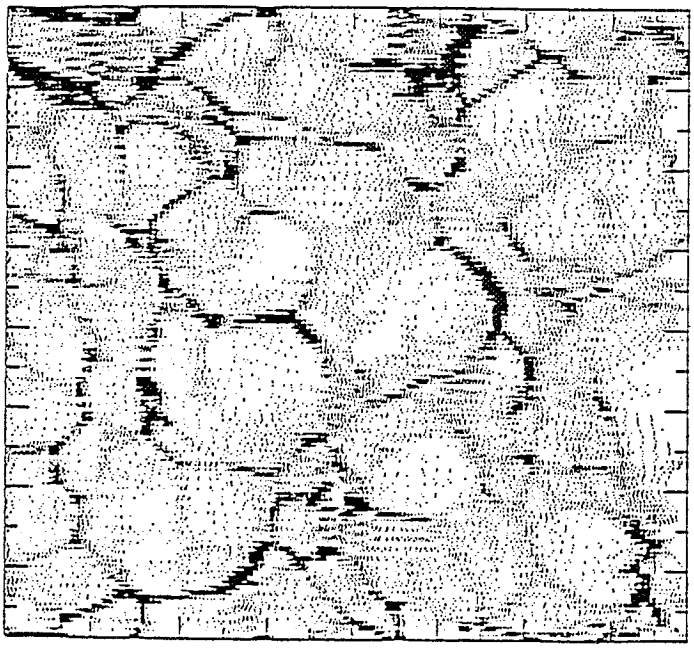

Fig. 3c

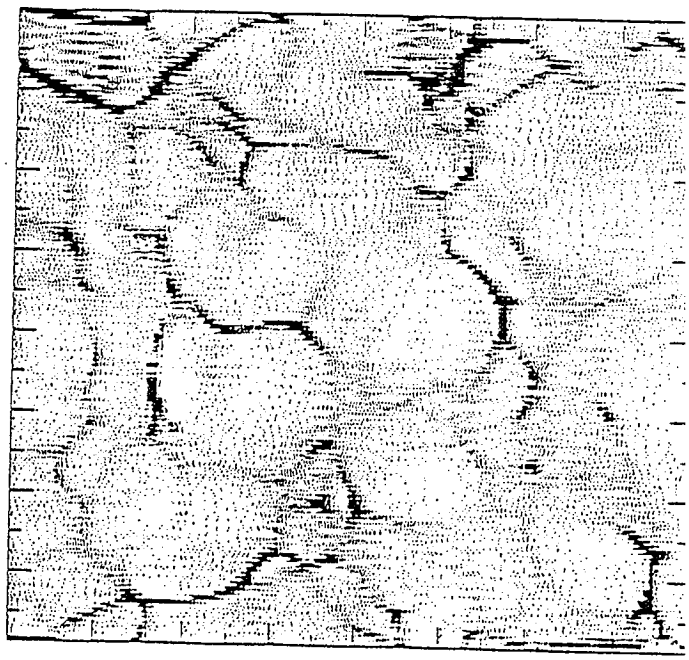

Fig. 3d

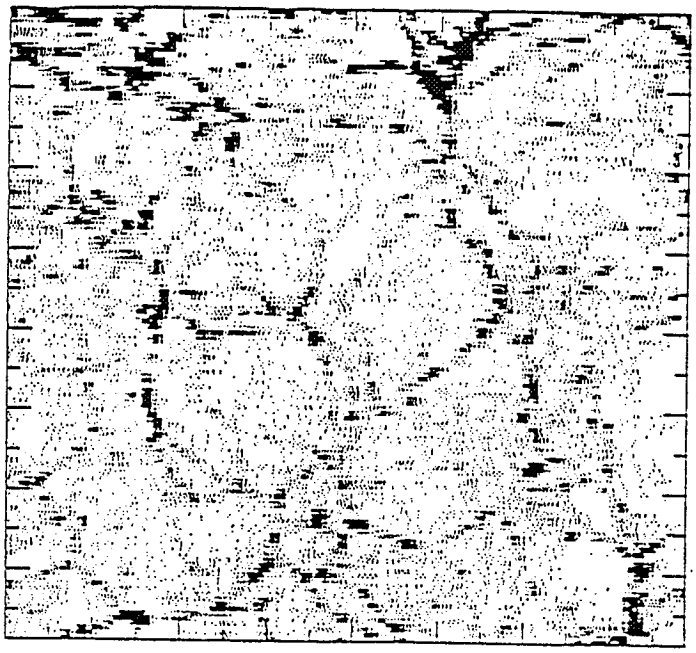

Fig. 4a

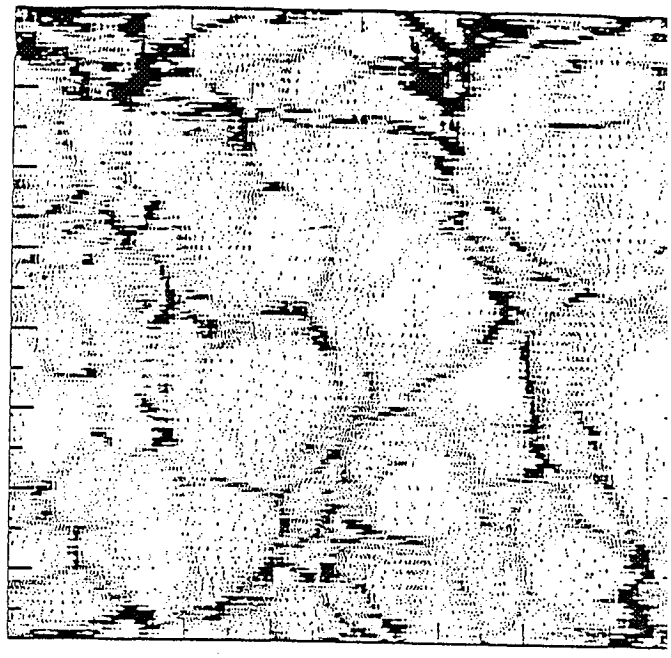

Fig. 4b

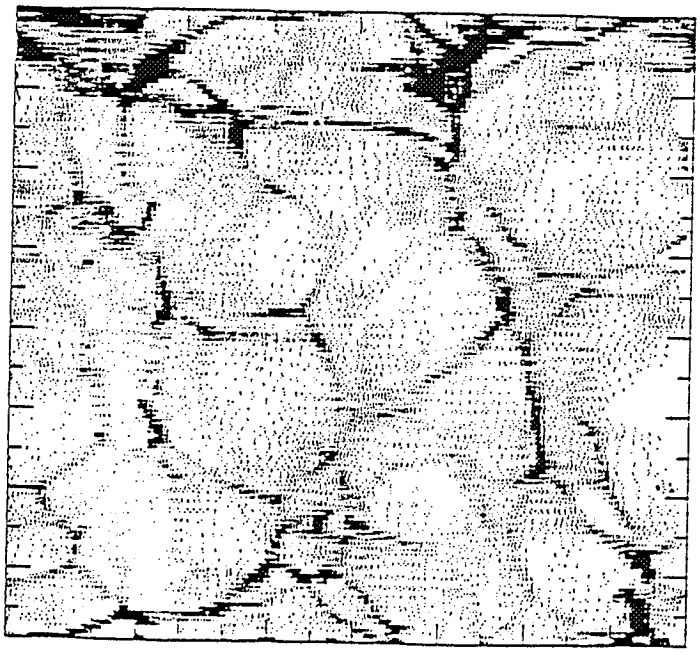

Fig. 4c

Fig. 4d

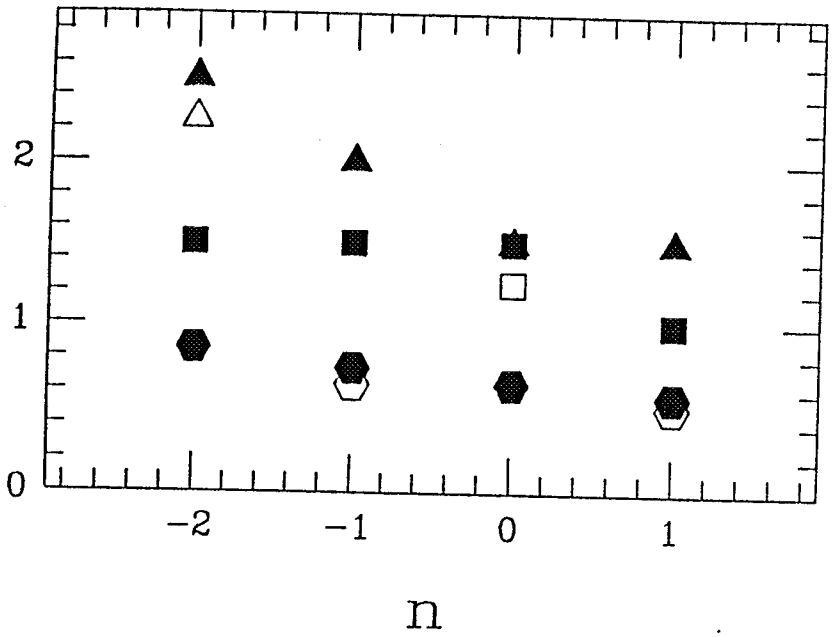

Fig. 5

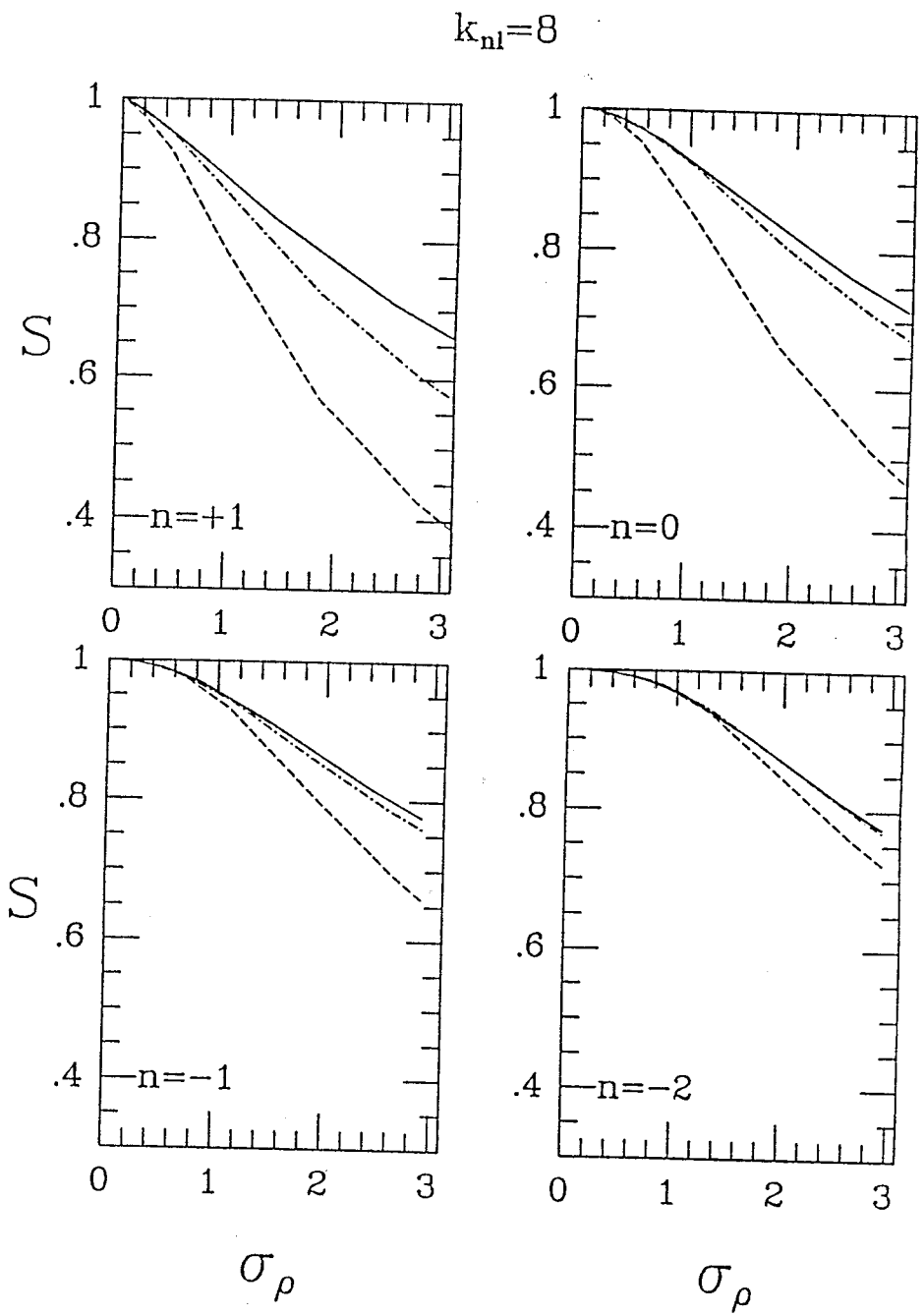

Fig. 6a

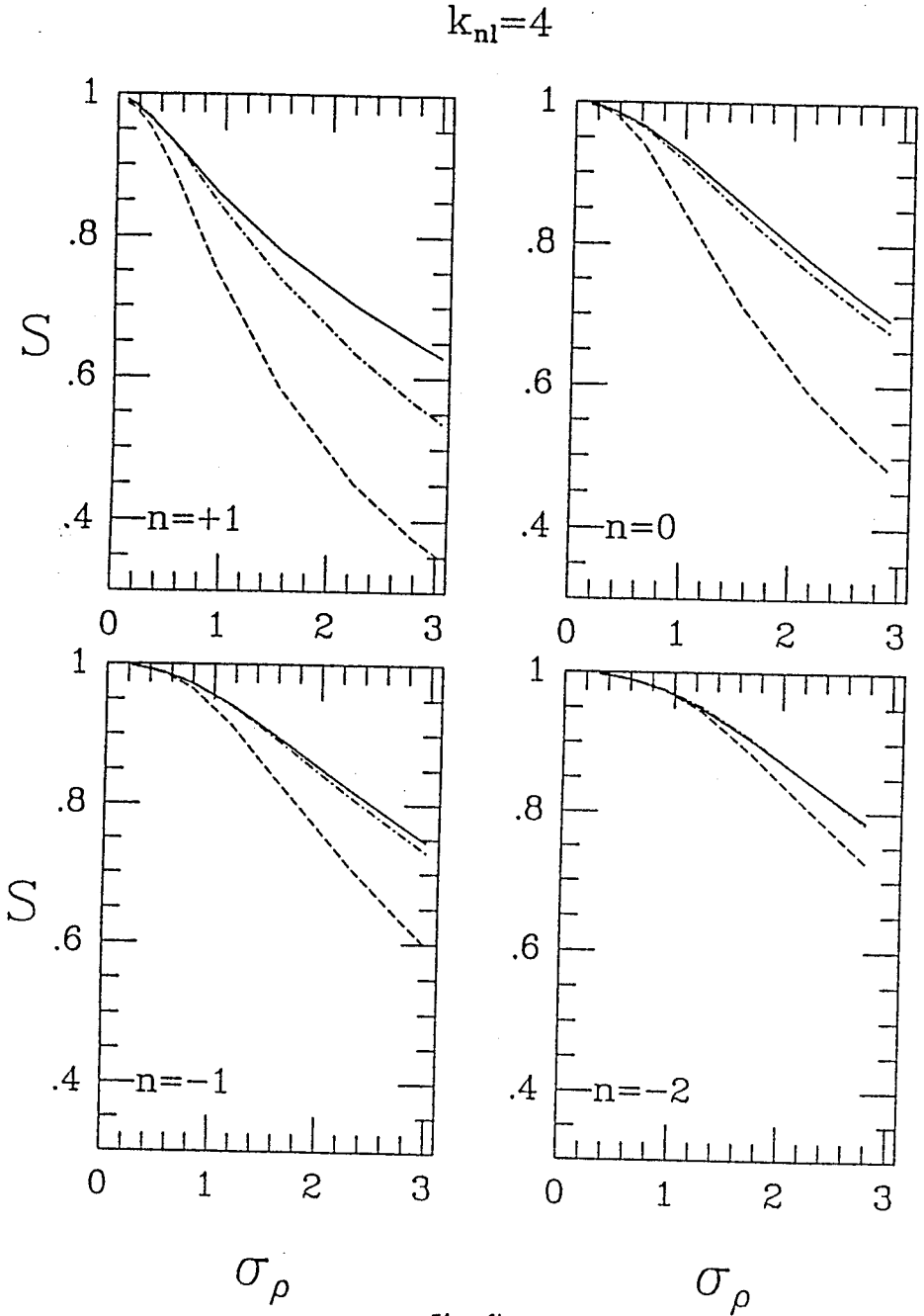
k_{nl}=4
S
n=+1
n=0
n=−1
n=−2
σ_ρ
σ_ρ

Fig. 6b

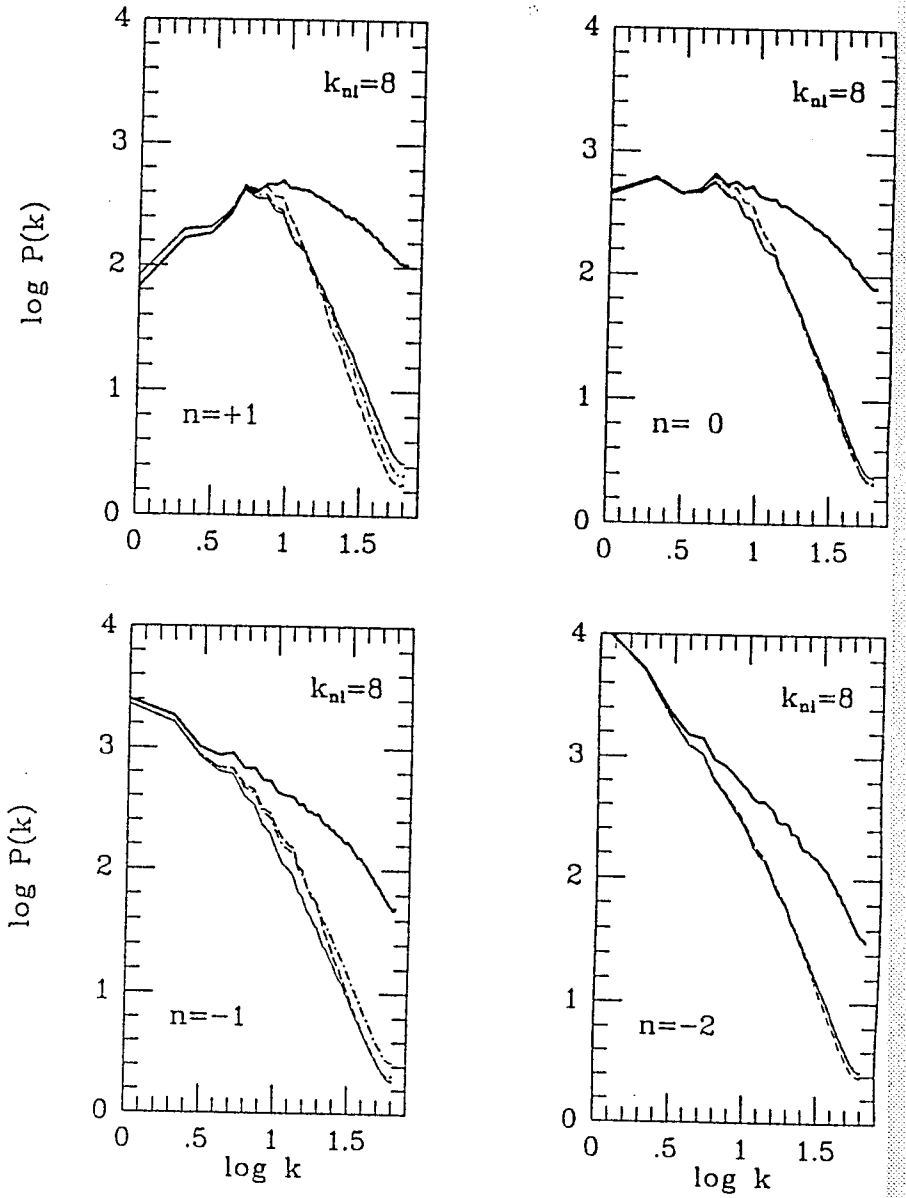
log P(k)
k_{nl}=8
n=+1
n= 0
n=−1
n=−2
log k
log k

Fig. 7

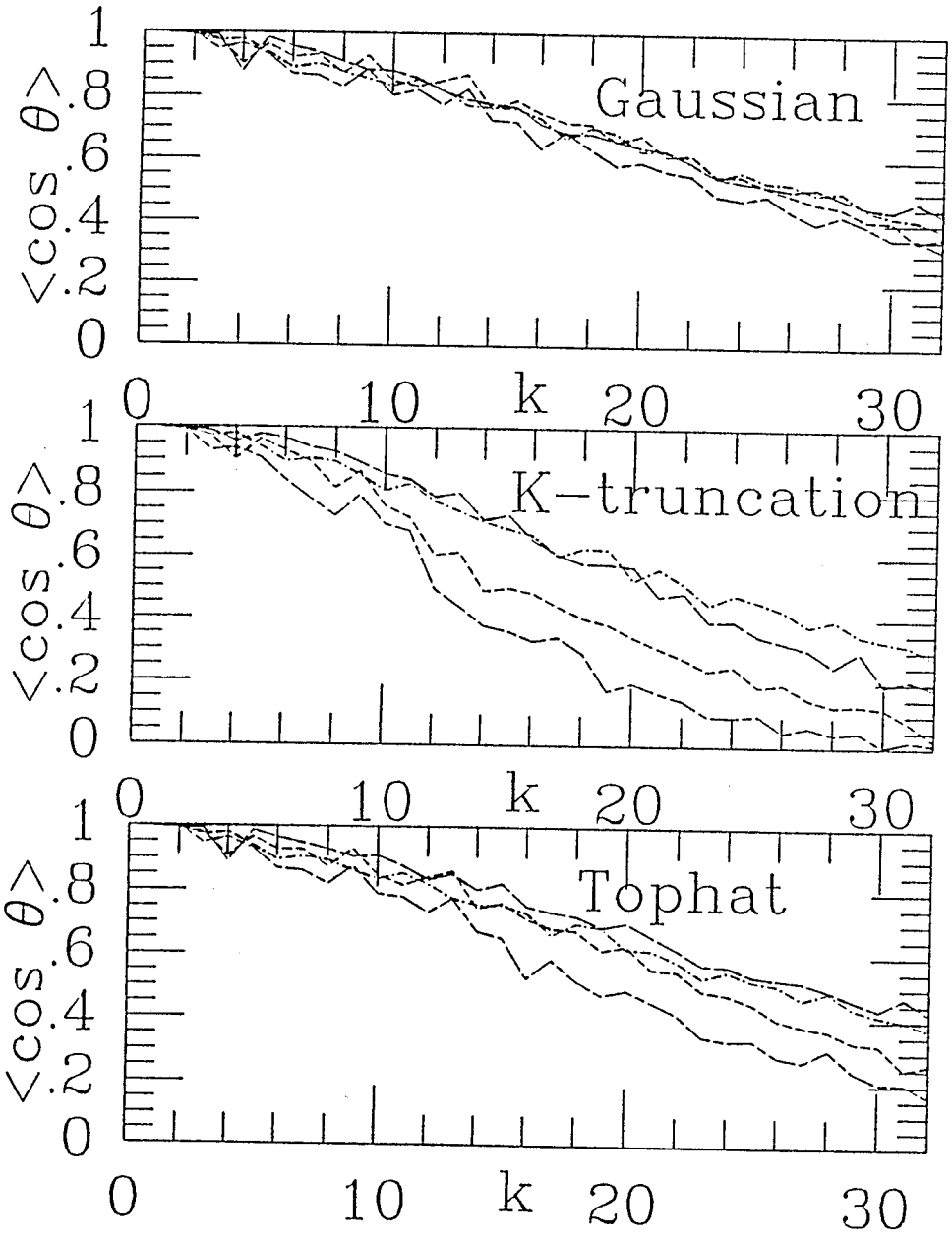
Gaussian
K-truncation
Tophat
<cos θ>
k
0
10
20
30
.2
.4
.6
.8
1

Fig.8

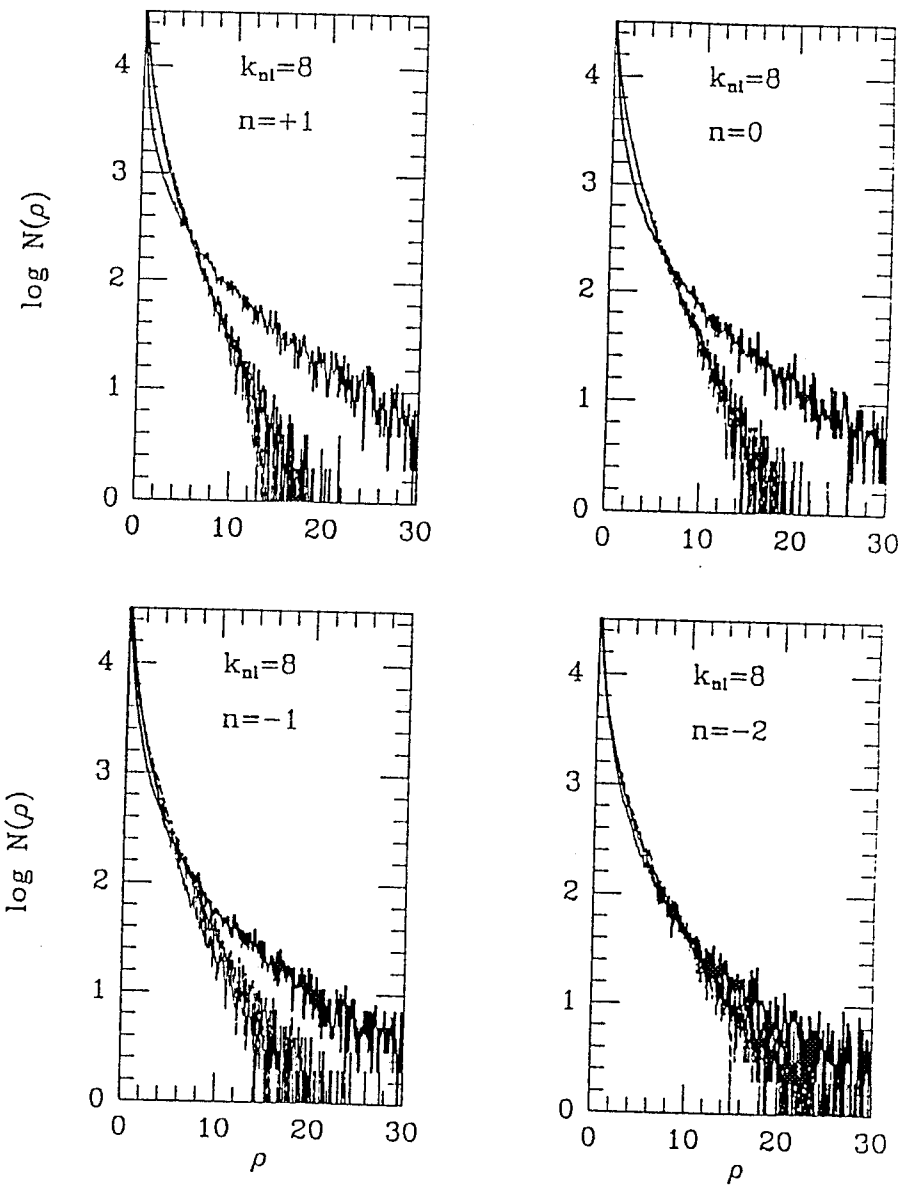
log N(ρ)
ρ
k_nl=8
n=+1
n=0
n=−1
n=−2
0
1
2
3
4
10
20
30

Fig. 9

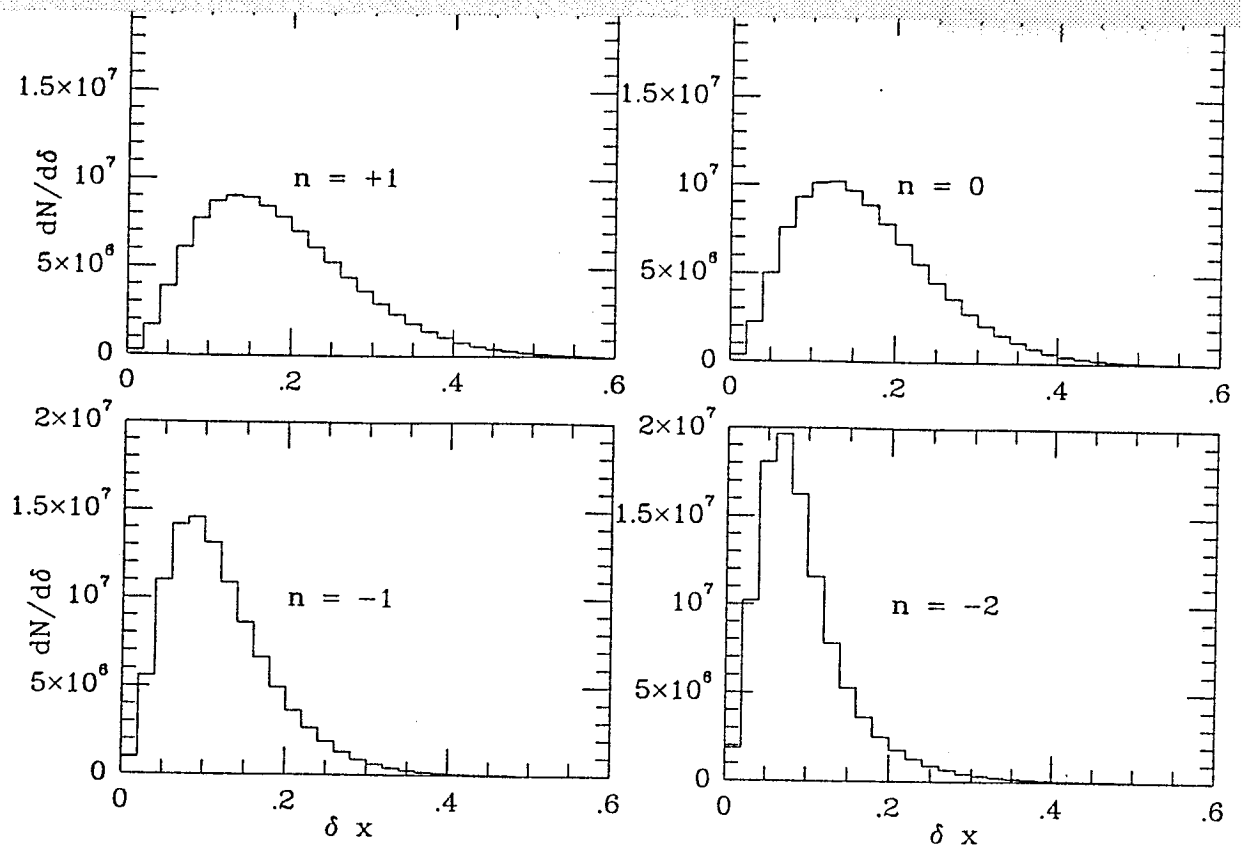

Figure 10

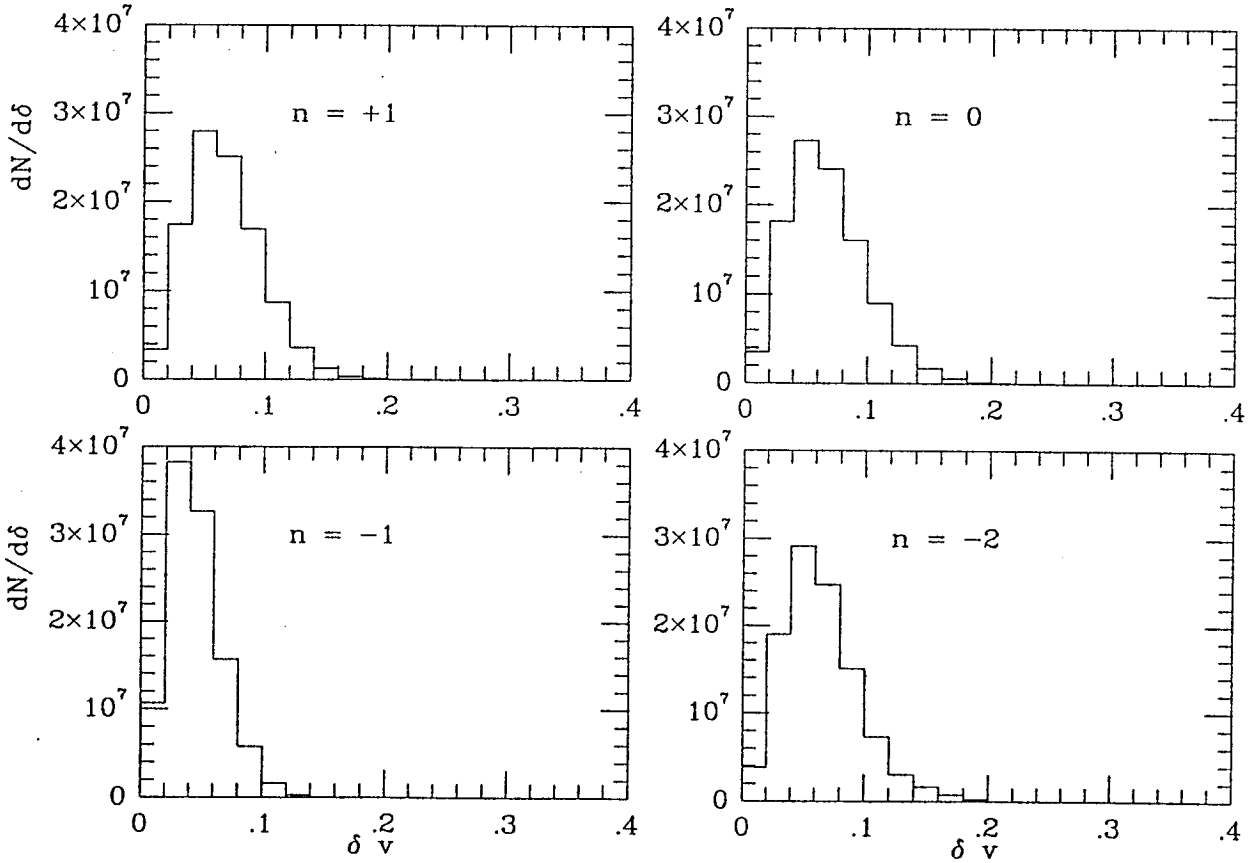

Figure 11